Sustainable Energy, Grids and Networks 26 (2021) 100418

Contents lists available at ScienceDirect

Sustainable Energy, Grids and Networks

journal homepage: www.elsevier.com/locate/segan

Resilient-enhancing critical load restoration using mobile power sources with incomplete information

Seyed Amin Sedgh [a], Meysam Doostizadeh [b], Farrokh Aminifar [a,c,*], Mohammad Shahidehpour [c]

[a] School of Electrical and Computer Engineering, College of Engineering, University of Tehran, 1555634414, Iran
[b] Faculty of Engineering, Lorestan University, Khorramabad, 6815144316, Iran
[c] Electrical and Computer Engineering Department, Illinois Institute of Technology, Chicago, IL 60616, USA

ARTICLE INFO

Article history:
Received 19 June 2020
Received in revised form 16 November 2020
Accepted 3 December 2020
Available online 12 January 2021

Keywords:
Microgrid
Mobile power sources
Resilience
Two-stage robust optimization

ABSTRACT

Mobile power sources (MPSs) have great potentials to enhance the resilience of distribution system due to mobility and flexibility. However, because of incomplete and asynchronous data after a natural disaster, decisions may lead to under-utilization of MPS and weak recovery performance. This paper proposes a robust receding horizon recovery strategy that dispatches MPSs and forms multiple microgrids (MGs) to maximize the restored critical loads (CLs). The receding horizon framework is utilized to update the system information dynamically and re-optimize the problem until accomplishment of the recovery process. A two-stage robust optimization formulation is adopted to take into account the problem uncertainty, i.e. unknown status of branches in damaged areas. Due to long-lasting duration of the recovery process, charging capability for re-chargeable MPSs is added to the proposed approach. Several case studies are carried out on IEEE 33-node distribution test system and IEEE 123-node test feeder to verify the effectiveness of proposed framework. The benefits of the new model are remarkable when there is a significant level of incomplete information, which is a likely case after high impact natural disasters.

1. Introduction

Natural disasters over the last years have triggered significant power outages with high-impact and long-lasting effects [1]. The catastrophic consequences for the economy and society have underlined the significance to reinforce power system resilience [2]. Since distribution systems remain in danger in the case of natural events and could leave numerous customers without electricity for days, immediate and effective response is one of crucial requirements of a resilient distribution system [3]. As conventional recovery strategies cannot restore loads fast enough [4], distribution systems would require an enhanced strategy for resilience. Microgrids (MGs) not only enhance the level of social welfare and the reliability of distribution systems [5–7], but also are deemed as one of the prominent solutions to boost the resilience of distribution systems [8,9]. Ref. [10] introduced a hierarchical scheme for outage management in a smart grid with multiple MGs. In [11], an advanced distribution system recovery method was proposed to restore critical loads (CLs). The method optimally allocates available distributed energy resources to CLs and forms resilient MGs.

Mobile power sources (MPSs) offer spatiotemporal mobility for immediate electrical service restoration over distribution systems [4]. This feature is particularly attractive when customers have partial access to the main grid, which is prevalent in natural disasters [12]. A two-stage MPS positioning framework was introduced in [12], consisting of pre-positioning and real-time allocation of resources. The charging capability is excluded in this work. Ref. [13] proposed a novel method for the adaptive formation of multi-MGs as one of the operational features for improving the critical service restoration strategy. Nonetheless, the model is not multi-period and MPSs are dispatched once at the first stage of disasters. Therefore, it is unable to fully utilize the MPS versatility and flexibility. In [14], a combined post-disaster load restoration strategy was developed for MPS pre-positioning and routing, MG generation scheduling, and grid reconfiguration. Ref. [15] introduced a resilient scheme for post-disaster recovery logistics that include network reconfiguration, coordinating repair crews, and MPSs. Ref. [16] investigated a load restoration framework that would optimize the dispatch of MPSs and the travel times of repair crews.

* Corresponding author at: Electrical and Computer Engineering Department, Illinois Institute of Technology, Chicago, IL 60616, USA.
E-mail addresses: amin.sedgh@ut.ac.ir (S.A. Sedgh), doostizadeh.me@lu.ac.ir (M. Doostizadeh), faminifar@ut.ac.ir (F. Aminifar), ms@iit.edu (M. Shahidehpour).

https://doi.org/10.1016/j.segan.2020.100418
2352-4677/

Nomenclature

A. Indices

i, j	Indices of nodes.
k	Index of MPSs.
l, m, u	Indices of station nodes for MPS positioning.
t	Index of time.
z	Index of unknown zones.

B. Sets

$\mathcal{B}$	Set of stations for MPS connection.
$\mathcal{DL}$	Set of nodes connected by damaged branches.
$\mathcal{F}_{i,j}^{l}$	Set of parents i and their offspring j regarding station l.
$\mathcal{G}$	Set of nodes.
$\mathcal{G}_z$	Set of nodes in unknown zone z.
$\mathcal{L}_z$	Set of branches in unknown zone z.
$\mathcal{M}$	Set of MPSs.
$\mathcal{T}_{ij}$	Set of estimated periods in which damaged branch ij is inoperable.
$\mathcal{T}_z$	Set of estimated inspection times of unknown zones.
$\mathcal{Z}$	Set of unknown zones.

C. Parameters

$CHL^k_{\max}/CHL^k_{\min}$	Maximum/minimum charge level of MPS k.
$P_{ch,k}$	Charging capacity of MPS k.
P^t_{imax}, Q^t_{imax}	Active/reactive power demands of node i at time t.
P^k_{max}, Q^k_{max}	Maximum active/reactive power outputs of MPS k.
r_{ij}, x_{ij}	Resistance and reactance of branch ij.
s_{ijmax}	Apparent power capacity of branch ij.
T_M	Maximum estimated time horizon.
TT_{mu}	Travel time from station m to station n.
w^t_i, w^t_l	Binary, indicating whether node/station i/l is supplied by main grid or not.
α_i	Importance weight of load at node i.
η^c_k/η^d_k	Charging/discharging efficiency of MPS k.
Π	A sufficiently large number.
Γ_z	Estimated maximum number of damaged branches in unknown zone z.
$\mathbf{A}/\mathbf{c}$	Outer level matrices/vector of coefficients.
$\mathbf{B}/\mathbf{f}$	Coefficient matrices/vector of mid-level.
$\mathbf{D}, \mathbf{E}, \mathbf{G}, \mathbf{J}, \mathbf{H}, \mathbf{M}, \mathbf{N}/\mathbf{b}, \mathbf{e}$	Inner level matrices/vectors of coefficients.

D. Variables

CHL^t_k	Charging level of MPS k at time t.
$D^{k,t}_l$	Binary, 1 if MPS k is positioned in station l at time t.
$P^{l,t}_i/Q^{l,t}_i$	Restored active/reactive power demands of node i by station l at time t.
$pf^{l,t}_i/qf^{l,t}_i$	Active/reactive in-flow powers of node I corresponding to MG l at time t.
u_{ij}	Binary, 1 if branch ij is undamaged.
$V^{l,t}_i$	Voltage of node i powered by station l at time t.
$v^{l,t}_i$	Binary, 1 if node i belongs to station l at time t.
x^t_k	Binary, 1 if MPS k is being charged at time t.

Uncertainties in real time operations could have a major impact on the resilience enhancement problem. In [4], an innovative two-stage framework was introduced, in which a robust optimization model is used to pre-position MPSs at the first stage (ex-ante) to improve the system survivability. At the second stage (ex-post), MPSs are dispatched and network topology is reconfigured under the assumption of complete information about the damages. This assumption might not hold in prevailing disasters. Ref. [17] introduced a stochastic post-hurricane recovery framework that uses both MPSs and reconfiguration plan to improve the resilience of networked MGs. The uncertain parameters include MPS travel times and active/reactive load demand; the status of branches in damaged areas are however considered to be known right after the event.

Using the Monte Carlo simulation method, uncertainties representing the status of roads, branches, and load demands were captured by scenario trees in [18]. However, calculating the probability of each scenario, due to the lack of sufficient historical data pertaining to natural disasters, is hardly possible. An innovative approach was proposed in [19] to tackle the uncertainties of switches status and asynchronous information during the distribution system recovery process. However, the incorporated energy sources are not mobile and this feature notably restricts the problem flexibility.

Another essential facet of the ex-post load restoration problem is the dynamic nature of field data. After a disaster, various types of field data [18], which are employed in order to enhance the restoration performance, needs to be updated progressively for the real-time decision-making.

In the light of literature review, there is a research gap to model the dynamic nature of field data and uncertainty of branches status in damaged zones during the distribution system recovery process. For this purpose, a robust receding horizon based recovery process is proposed in this paper. The proposed recovery process optimally dispatches MPSs and forms MGs to maximize the restored CLs in a resilient distribution system. In order to manage the uncertainty of branches status in damaged areas of distribution network, a two-stage robust optimization method is devised. Since the decisions are immunized against the worst-case scenario, the final recovery process is utterly robust for the given uncertainty budget. Furthermore, a receding horizon framework is adopted to exploit the progressively updated data in the favor of solution optimality. This framework continuously updates the unknown status of branches and re-optimizes the decisions to restore more CLs. The charging capability of mobile energy storage systems is also incorporated in the model to enhance the flexibility of recovery process. Accordingly, the major contributions of this paper are as follows:

- In order to optimally dispatch MPSs and form multiple optimal MGs after the natural disaster, the uncertainty of branches status in damaged areas of distribution system is managed by a two-stage robust optimization model.
- A receding horizon framework is applied to exploit the gradually updated branches status data in damaged areas. This framework re-optimizes the decisions after field crew's inspections so as to restore more weighted CLs.

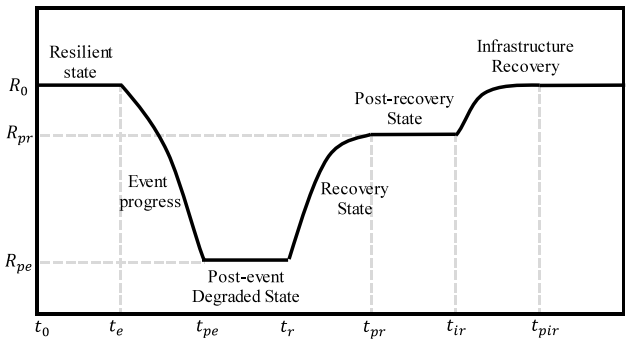

Fig. 1. Conceptual resilience curve associated with an event.

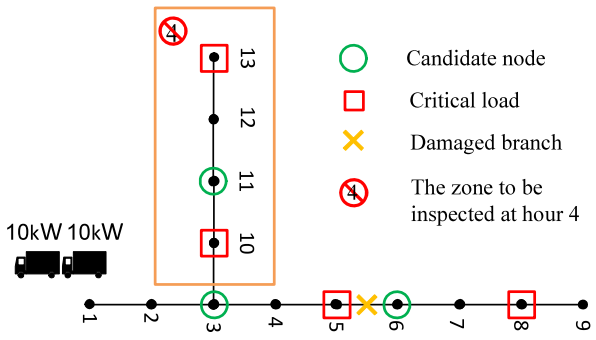

Fig. 2. An illustrative example to show post-disaster hard decision-making.

2. Proposed problem statement

Fig. 1 illustrates a typical resilience curve following to an event [18]. R refers to a system performance metric. System states include resilient pre-event state (t_0, t_e), event progress (t_e, t_{pe}), degraded post-event state (t_{pe}, t_r), recovery state (t_r, t_{pr}), post-recovery state (t_{pr}, t_{ir}), and infrastructure recovery (t_{ir}, t_{pir}).

As recovery state starts at t_r, DSO schedules resources and forms multiple MGs [1]. Due to credible damages to the monitoring system or its original limited coverage, the status of network branches are just partially known at the beginning of the recovery process. So, inspection is needed to realize the status of branches in zones with incomplete information. DSO dispatches crews toward these *unknown zones* to gradually specify the status of branches and update the damage databases. MPSs can then form MGs to restore intact CLs located in those zones. It should be emphasized that the electricity network is the only part exposed to the event and CLs themselves are assumed intact and needing electricity as much as ex-ante.

For clarification of uncertainty impacts, a simple example is represented in Fig. 2. There is an unknown zone depicted by a rectangular box and a known damaged branch between Nodes 5 and 6. According to the field crews' declared plan, the status of branches in the unknown zone will be identified 4 h later, and the respective CLs can be then restored. There are 2 similar MPSs with 10 kW power capacity and 4 CLs, with equal importance except CL 10, which is much more critical than the others. Each CLs demand is 6 kW. Suppose that DSO does not take into account the uncertain branches status and wants to maximize the restored CLs amount at each time. It dispatches 2 MPSs toward candidate Nodes 3 and 6. So, CLs 5 and 8 are restored by MPSs 1 and 2, respectively. DSO hopes that MPS 1 will pick up two other CLs after the zone inspection. However, if the branch between Nodes 3 and 10 is damaged, the DSO will not be able to pick them up. Even if the branch is declared intact, the MPS 1 does not have enough capacity to fully pick CL 10 up. Since CL 10 is more critical than 5, the DSO's decisions are not optimal in a long-lasting horizon. If DSO had sent MPS 1 to Node 11 at the beginning of the recovery state, the greater sum of weighted CLs would have been served.

In summary, to optimally allocate the resources, the DSO should consider distribution system topology including uncertainty of branches status, field crews' schedule, MPSs characteristics, and CLs priorities and demands. Moreover, in order to have higher restored CLs, DSO should update the data during the recovery process and re-optimize decision variables over the remaining periods. It should be also emphasized that, in the power system recovery, it is not common to interrupt a CL after the pick up [19]. Therefore, at the beginning of the recovery state at t_r, the DSO is faced with incomplete data that will be updated, dynamically.

3. Proposed model

The objective function in this paper is maximizing the sum of weighted restored CLs. The proposed multi-period two-stage robust optimization formulation identifies branches of unknown zones with the worst effect on the objective function. Using the proposed formulation, the DSO can dynamically schedule MPSs and form MGs, while taking the uncertainty of branches status in unknown zones into account. At first, the proposed formulation is presented for a specific time duration of the recovery process. Then, the model is developed to a receding horizon recovery framework so that it utilizes this two-stage robust optimization formulation and re-optimizes the decisions. The receding horizon framework will be presented in Section 4.

3.1. Mathematical formulation

The goal is to maximize the total of restored weighted CLs under the worst-case scenario of the recovery process horizon. The tri-level objective function is stated as follows:

$$\max_{D_k^{l,t},v_i^{l,t},x_k^t}\ [\min_{u_{ij}}(\max_{P_i^{l,t},pf_i^{l,t},qf_j^{l,t},V_i^{l,t},CHL_k^t}\sum_t\sum_i\sum_l \alpha_i P_i^{l,t})] \tag{1}$$

In order to clearly present the different decision variables and constraints of each level, the outer, mid and inner levels of the proposed tri-level optimization model are demonstrated separately in (2), (3) and (4), respectively [20].

The outer level (2) determines the optimal MPSs scheduling (i.e., $D_k^{l,t}$ and x_k^t) and multiple MGs formation (i.e.,$v_i^{l,t}$). The objective function (2a) maximizes the total of restored CLs under the worst-case scenario.

$$\max_{D_k^{l,t},v_i^{l,t},x_k^t}\ \phi \tag{2a}$$

Subject to:

$$\frac{1}{2}\sum_{k\in\mathcal{M}} D_l^{k,t} \le v_i^{l,t} \qquad i=l,\forall l,\forall t \tag{2b}$$

$$\sum_{k\in\mathcal{M}} D_l^{k,t} \ge v_i^{l,t} \qquad \forall i,\forall l,\forall t \tag{2c}$$

$$\sum_{l\in\mathcal{B}} D_l^{k,t} \le 1 \qquad \forall k,\forall t \tag{2d}$$

$$\sum_{l\in\mathcal{B}} v_i^{l,t} \le 1 \qquad \forall i,\forall t \tag{2e}$$

$$v_j^{l,t} - v_i^{l,t} \le 0 \qquad \forall (i,j,l)\in\mathcal{T}_{i,j}^l,\forall t \tag{2f}$$

$$v_i^{l,t} + v_j^{l,t} \le 1 \qquad \forall\,(i,j)\in\mathcal{DL},\forall t\in\mathcal{T}_{ij} \tag{2g}$$

$$D_m^{k,t+n} + D_u^{k,t} \le 1 \qquad \forall k,\forall m,\forall u,\forall n\le TT_{mu}\forall t+n\le T_M \tag{2h}$$

$$v_i^{l,t} = 0 \qquad \forall l, \forall i \in \mathcal{G}_z, \forall t \in \mathcal{T}_z \quad (2i)$$

$$x_k^t \le \sum_{l \in \mathcal{B}} D_l^{k,t} \times w_l^t \qquad \forall k, \forall t \quad (2j)$$

$$v_i^{l,t} \le 1 - w_i^t \qquad \forall l, \forall i, \forall t \quad (2k)$$

Constraint (2b) states that if at least 1 MPS is positioned at station l in node i, then node i must be energized by that station (i.e., $v_l^{l,t} = 1$). This equation also limits the number of MPSs at each station, which is 2 here. Constraint (2c) states that each node can be supplied by station l, if the station has at least 1 MPS. Constraint (2d) ensures that every MPS is placed exactly at 1 station at each time. Constraint (2e) imposes that each node can be picked up by only 1 MPS. Constraint (2f) must be met to retain the MG radial topology. It states that a node can be a member of an MG only if its parent node is a member of that MG. This is because in a radial topology, each MG is supposed to be a sub-tree network of energized nodes in which its root is a power source node. Constraint (2g) states that if branch ij is declared damaged, the corresponding nodes cannot be a member of the same MG before repairing the damaged branch.

Constraint (2h) characterizes the MPS transportation and ensures the required traveling time for MPS transportation [4]. For instance, if relocating MPS 1 from Node 4 to Node 3 takes 2 h, Node 3 cannot host MPS 1 within the next 2 h. Under this circumstance, constraint (2h) becomes as follows:

$$D_3^{1,t+1} + D_4^{1,t} \le 1 \quad \forall t+1 \le T_M$$

$$D_3^{1,t+2} + D_4^{1,t} \le 1 \quad \forall t+2 \le T_M$$

Consequently, $D_3^{1,t+1}$ and $D_3^{1,t+2}$ are forced to be 0 if $D_4^{1,t} = 1$.

Constraints (2i)–(2k) model the declared field crews' schedule. Since CLs are inoperable during the estimated inspection time$(\mathfrak{T}_3)$, energizing the nodes locating in unknown zone z are constrained by (2i). Constraint (2j) states that if the upstream substation energizes a station at time t (i.e., $w_l^t = 1$), its respective MPS can be charged. This equation enables the charging capability of mobile energy storage systems. Similarly, constraint (2k) states that if a node is served by the upstream substation at time t (i.e., $w_i^t = 1$), it should not be picked up by any MPS. Note that w_l^t and w_i^t are binary parameters, set by field crews' plan.

Given the outer level decision variables, the mid-level (3) finds the worst-case branch damage scenario over all uncertain branches. The objective function (3a) optimally determines the set of uncertain branches (u_{ij}) that minimize the total of restored weighted CLs of the inner level. Constraint (3b) outlines the assumption that the number of damaged branches in unknown zone z will not be more than a particular Γ_z which is already specified. Ref. [4] has proposed an innovative method to set this parameter. By changing this parameter, the DSO can adjust the conservativeness of the model.

$$\phi = \min_{u_{ij}} \Delta \quad (3a)$$

Subject to:

$$\sum_{(i,j) \in \mathcal{L}_\mathcal{Z}} \left(1 - u_{ij}\right) \le \Gamma_z \quad (3b)$$

Per outer level decisions and mid-level damage results, the total of restored weighted CLs is maximized in the inner level (4). Regarding the obtained outer and mid-level decision variables, the objective function (4a) seeks to find the optimal decision variables $P_i^{l,t}$, $pf_i^{l,t}$, $qf_j^{l,t}$, $V_i^{l,t}$ and CHL_k^t that maximize the total of restored weighted CLs. The priority of CLs is taken into account by the parameter α_i in the objective (4a). By adjusting this parameter, the DSO is able to not only capture the priority of CLs in the model, but also discriminates various CLs appropriately. Note that, at recovery state (t_r, t_{pr}), the DSO sets the weights of non-critical loads to zero. Therefore, the objective function maximizes the weighted restored CLs, and the model selects the choice with highest worst-case objective value.

$$\Delta = \max_{P_i^{l,t}, pf_i^{l,t}, qf_j^{l,t}, V_i^{l,t}, CHL_k^t} \sum_t \sum_i \sum_l \alpha_i P_i^{l,t} \quad (4a)$$

Subject to:

$$pf_i^{l,t} = P_i^{l,t} + \sum_{j \in \mathcal{F}_{i,j}^l} pf_j^{l,t} \qquad \forall i, \forall l, \forall t \quad (4b)$$

$$qf_i^{l,t} = Q_i^{l,t} + \sum_{j \in \mathcal{F}_{i,j}^l} qf_j^{l,t} \qquad \forall i, \forall l, \forall t \quad (4c)$$

$$0 \le pf_i^{l,t} \le \Pi \times \sum_{k \in \mathcal{M}} D_l^{k,t} \qquad \forall i, \forall l, \forall t \quad (4d)$$

$$0 \le qf_i^{l,t} \le \Pi \times \sum_{k \in \mathcal{M}} D_l^{k,t} \qquad \forall i, \forall l \forall t \quad (4e)$$

$$0 \le P_i^{l,t} \le P_{imax}^t \times v_i^{l,t} \qquad \forall i, \forall l, \forall t \quad (4f)$$

$$Q_i^{l,t} = \left(\frac{Q_{imax}^t}{P_{imax}^t}\right) \times P_i^{l,t} \qquad \forall i, \forall l, \forall t \quad (4g)$$

$$P_i^{l,t} - P_i^{l,t+1} \le 0 \qquad \forall i, \forall l, \forall t \quad (4h)$$

$$\begin{aligned} &\left(\sum_{k \in \mathcal{M}} D_l^{k,t} - 1\right)\left(2 - \sum_{k \in \mathcal{M}} D_l^{k,t}\right)\Pi \\ &\quad + V_{ref} \le V_i^{l,t} \\ &\le V_{ref} + \left(1 - \sum_{k \in \mathcal{M}} D_l^{k,t}\right) \\ &\quad \times \left(2 - \sum_{k \in \mathcal{M}} D_l^{k,t}\right)\Pi \end{aligned} \qquad i = l, \forall t \quad (4i)$$

$$V_j^{l,t} = V_i^{l,t} - \frac{r_{ij} pf_j^{l,t} + x_{ij} qf_j^{l,t}}{V_{ref}} \qquad \forall (i,j,l) \in \mathcal{F}_{i,j}^l, \forall t \quad (4j)$$

$$0.95 \le V_i^{l,t} \le 1.05 \qquad \forall i, \forall l, \forall t \quad (4k)$$

$$\sum_{i \in \mathcal{G}} P_i^{l,t} \le \sum_{k \in \mathcal{M}} D_l^{k,t} \times P_{max}^k \qquad \forall l, \forall t \quad (4l)$$

$$\sum_{i \in \mathcal{G}} Q_i^{lt} \le \sum_{k \in \mathcal{M}} D_l^{k,t} \times Q_{max}^k \qquad \forall l, \forall t \quad (4m)$$

$$pf_j^{l,t2} + qf_j^{l,t2} \le s_{ijmax}^2 \qquad \forall (i,j,l) \in \mathcal{F}_{i,j}^l, \forall t \quad (4n)$$

$$pf_j^{l,t} \le \Pi \times u_{i,j} \qquad \forall (i,j,l) \in \mathcal{F}_{i,j}^l, \forall t \quad (4o)$$

$$qf_j^{l,t} \le \Pi \times u_{i,j} \qquad \forall (i,j,l) \in \mathcal{F}_{i,j}^l, \forall t \quad (4p)$$

$$CHL_{min}^k \le CHL_k^t \le CHL_{max}^k \qquad \forall k, \forall t \quad (4q)$$

$$\begin{aligned} CHL_k^{t+1} = CHL_k^t + \frac{\Delta T\left(x_k^t \times P_{ch,k}\right)}{\eta_k^d} \\ -\Delta T \times \eta_k^c \left(\sum_{l \in \mathcal{B}} D_l^{k,t} \sum_{i \in \mathcal{G}} P_i^{l,t} \times \right. \\ \left. \left(1 - \sum_{k' \ne k} \left(\frac{P_{max}^{k'}}{P_{max}^{k'} + P_{max}^k}\right) D_l^{k',t}\right)\right) \end{aligned} \qquad \forall k, \forall t \quad (4r)$$

Constraints (4b) and (4c) represent nodal active and reactive power balances, as stated by DistFlow model [12]. Constraints (4d) and (4e) enforce the in-flow powers of node i pertaining to station l to be 0 if there is no MPS in this station; otherwise, they are relaxed. Constraint (4f) states that if a CL is picked up by a station, the active power should not exceed CLs maximum active demand; otherwise, it is 0. The ratio of active and reactive

demands of CLs is taken into consideration in (4g). In fact, it is assumed that the power factors of power demands are fixed. Constraint (4h) states that once a CL is picked up, the served demand cannot be de-energized or even reduced. The voltage of a candidate node (station) is set to be 1 p.u. if it has at least 1 MPS installed, (4i). Otherwise, this constraint is relaxed. The voltages at other nodes of MG supplied by station l are given in (4j), based on DistFlow model. Constraint (4k) limits the voltage magnitude. Inequalities (4l) and (4m) indicate that the sum of CLs being supplied by MPS k located in station l should be capped by its associated capacities. Constraint (4n) provide the branch capacity limitations. Active and reactive power flows on damaged branches should be 0, (4o) and (4p). Constraint (4q) limits the charge level of MPSs between standard ranges. Finally, Eq. (4r) presents MPS charge level variations over the time. It is worth noting that constraints (4n) and (4r) are non-linear. Accordingly, an effective technique proposed in [21] is used to linearize (4n). Also, the bi-linear terms in (4r) is linearized based on a method presented in [4].

4. Scheme overview and solution methodology

The outline of the proposed multi-period robust receding horizon-based recovery is shown in Fig. 3. It is consisting of three main stages, initialization, preparation, and receding horizon recovery process. In the first stage, which is before the event, distribution system configuration data, CL demand and priorities, MPSs characteristics and locations are initialized. Proactive management, such as pre-positioning of MPSs and line hardening, can be considered at this stage. Ref. [22] have proposed effective approaches to improve the survivability of the distribution network before the event. At the second post-event stage, multiple sources of data are used to determine faults and damages in the distribution system. The damaged branches, unknown zones, field crews' schedule, and the maximum estimated time duration of recovery process are determined and used in the next stage. The field crews' schedule specifies estimated zones inspection times and repair times of certain damaged branches.

At the third stage, the two-stage robust optimization problem is solved over the estimated horizon of the recovery process. The process of solving this problem is presented in Fig. 3. Then, the decisions (MPSs scheduling and MGs formations) are implemented only until the first zone inspection time. Then, the model is updated by the data associated with the inspection of the first zone. Considering the remaining uncertainties, the model is re-optimized and the decisions are implemented until the next zone inspection. This procedure continues until all uncertainty of branches status are cleared up completely. The last iteration in which there is no unknown zone will be implemented until the end of recovery process.

For succinct and explicit demonstration and analysis, the proposed tri-level "max–min–max" optimization model is presented in the following compact form:

$$\max_{r} \phi\,(\mathbf{r}, \mathbf{u}, \mathbf{q}) \tag{5a}$$

s.t.

$$\mathbf{Ar} \le \mathbf{c} \tag{5b}$$

$$\phi = \min_{u} \Delta\,(\mathbf{r}, \mathbf{u}, \mathbf{q}) \tag{5c}$$

$s.t.$

$$\mathbf{Bu} \le \mathbf{f} \tag{5d}$$

$$\Delta = \max_{q} \mathbf{b}^T\mathbf{q} \tag{5e}$$

$s.t.$

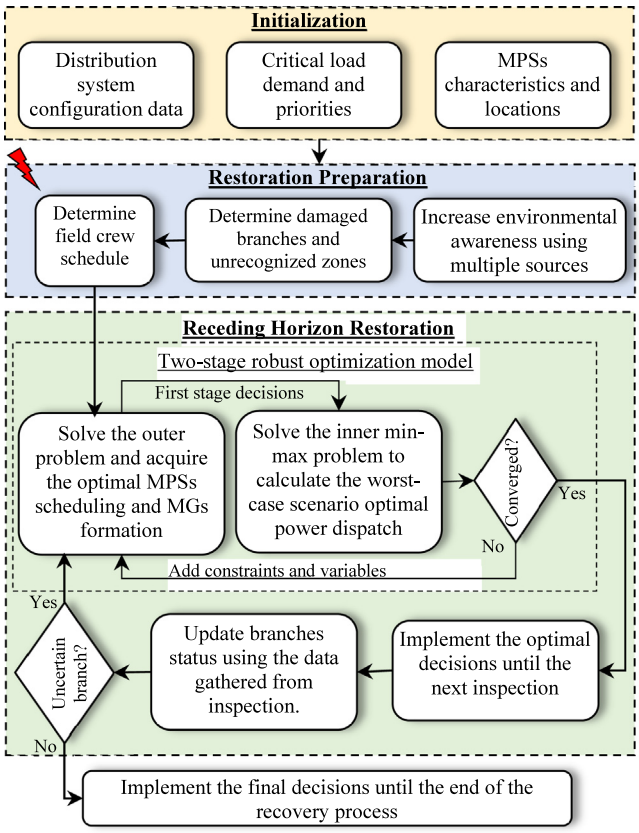

Fig. 3. Outline of the robust receding horizon-based recovery strategy.

$$\mathbf{Dq} \le \mathbf{e} \tag{5f}$$

$$\mathbf{Jq} = \mathbf{Hu} + \mathbf{Gr} \tag{5g}$$

$$\mathbf{Mq} \le \mathbf{Nu} + \mathbf{Er} \tag{5h}$$

where $\mathbf{r}$ is the vector of the outer level decision variables ($v_i^{l,t}$, $D_k^{l,t}$ and x_k^t), vector $\mathbf{u}$ denotes the uncertainty of branches status, and vector $\mathbf{q}$ represents the inner level decision variables ($P_i^{l,t}$, $pf_i^{l,t}$, $qf_j^{l,t}$, $V_i^{l,t}$ and CHL_k^t). Inequality (5b) indicates the outer level constraints (2b)–(2h) and (2j)–(2k) that are concisely written with matric $\boldsymbol{A}$ and right-hand-side vector $\mathbf{c}$. Note that equality (2i) is determined before running the optimization model since the DSO knows the nodes in unknown zones in advance. Constraint (5d) denotes the conservation level of the robust optimization. Accordingly, matric $\mathbf{B}$ and vector $\mathbf{f}$ are attained from (3b). Equality (5e) is the objective function for the inner problem, where vector $\mathbf{b}$ is obtained from (4a). Constraints (5f)–(5h) represent the inner level constraints defined in (4b)–(4r). Therefore, left-handed matric of coefficients $\mathbf{D}$ and right-handed vector of coefficients $\mathbf{e}$ are taken from (4h), (4k), (4n) and (4q). Also, matrices $\mathbf{J}$, $\mathbf{H}$ and $\mathbf{G}$ are obtained from (4b), (4c), (4g), (4j) and (4r), and matrices $\mathbf{M}$, $\mathbf{N}$ and $\mathbf{E}$ are derived from (4d)–(4f), (4i), (4l), (4m), (4o) and (4p).

At the time of writing, no available software package can solve this max–min–max formulation. The formulation can be separated into the following master and sub-problems, based on the robust two-stage optimization framework [23]. We then use the column and constraint generation (C&CG) algorithm to solve this two-stage robust optimization problem [24].

(1) Master problem: In order to figure out the optimum outer decision variables ($\mathbf{r}$) under the worst-case scenarios, the master problem is used. The worst-case scenarios ($\mathbf{u^n}$) are obtained

via the sub-problem at iteration n and are added to a subset of possible scenarios (O={$s_1, s_2, \ldots, s_n$}). The following master problem offers an upper bound for the two-stage robust formulation (5a)–(5h).

$$\max_{r,q(s)} \eta \tag{6a}$$

s.t

$$\eta \le \mathbf{b}^T \mathbf{q}^n(s) \qquad \forall s \in O \tag{6b}$$

$$\mathbf{Ar} \le \mathbf{c} \tag{6c}$$

$$\mathbf{Dq}^n(s) \le \mathbf{e} \qquad \forall s \in O \tag{6d}$$

$$\mathbf{Jq}^n(s) - \mathbf{Gr} = \mathbf{Hu}^n(s) \qquad \forall s \in O \tag{6e}$$

$$\mathbf{Mq}^n(s) - \mathbf{Er} \le \mathbf{Nu}^n(s) \qquad \forall s \in O \tag{6f}$$

Constraints (6d)–(6f) are similar to (5f)–(5h), while they are a function of the worst-case scenarios and have the iteration index n.

(2) Sub-problem: The following sub-problem can be achieved when a set of first stage variables $\mathbf{r}^*$ are specified.

$$\phi\left(\mathbf{r}^*, \mathbf{u}, \mathbf{q}\right) = \min_{u} \Delta\left(\mathbf{r}^*, \mathbf{u}, \mathbf{q}\right) \tag{7a}$$

s.t

$$\mathbf{Bu} \le \mathbf{f} \tag{7b}$$

$$\Delta\left(\mathbf{r}^*, \mathbf{u}, \mathbf{q}\right) = \max_{q} \mathbf{b}^T \mathbf{q} \tag{7c}$$

s.t

$$\mathbf{Dq} \le \mathbf{e} \qquad (\boldsymbol{\lambda}_1 \le 0) \tag{7d}$$

$$\mathbf{Jq} = \mathbf{Hu} + \mathbf{Gr}^* \qquad (\boldsymbol{\lambda}_2: \textit{free}) \tag{7e}$$

$$\mathbf{Mq} \le \mathbf{Nu} + \mathbf{Er}^* \qquad (\boldsymbol{\lambda}_3 \le 0) \tag{7f}$$

Since the above formulation is a "min–max" bi-level programming problem, it should be transformed into a single level "min" problem. To do so, we dualize the inner problem so it can merge with the mid-level problem. Therefore, the min–max sub-problem in (7a)–(7f) is converted into:

$$\phi\left(\mathbf{r}^*, \mathbf{u}, \mathbf{q}\right) = \min_{u,\boldsymbol{\lambda}_1,\boldsymbol{\lambda}_2,\boldsymbol{\lambda}_3} \mathbf{e}^T\boldsymbol{\lambda}_1 + \left(\mathbf{Hu} + \mathbf{Gr}^*\right)^T \boldsymbol{\lambda}_2 + \left(\mathbf{Nu} + \mathbf{Er}^*\right)^T \boldsymbol{\lambda}_3 \tag{7g}$$

s.t

$$\mathbf{Bu} \le \mathbf{f} \tag{7h}$$

$$\mathbf{D}^T\boldsymbol{\lambda}_1 + \mathbf{J}^T\boldsymbol{\lambda}_2 + \mathbf{M}^T\boldsymbol{\lambda}_3 \le \mathbf{b} \tag{7i}$$

$$\boldsymbol{\lambda}_1, \boldsymbol{\lambda}_3 \le 0, \boldsymbol{\lambda}_2: \textit{free} \tag{7j}$$

A lower bound to the original two-stage problem can be obtained by solving the sub-problem (7g)–(7j). The objective function (7g) comprises bi-linear terms of $\mathbf{u}\boldsymbol{\lambda}_2$ and $\mathbf{u}\boldsymbol{\lambda}_3$. Using the big M method, these terms can be linearized as stated in [21]. Finally, the CC&G algorithm is applied as presented in algorithm 1. The worst-case scenario for damaged branches ($\mathbf{u}^n$) is determined by setting optimal values for the first stage variables (r^{n*}). Then, this scenario is added to a subset of possible scenarios (O), and the first stage variables are updated. This iterative procedure will continue until the difference between upper and lower bounds is within a determined tolerance (ε).

Algorithm 1 C&CG Algorithm

1: **Set** $LB = -\infty$, $UB = +\infty$, $n = 1$, $\mathbf{u}^1 = 1$, $O = \varnothing$, and flag=no
2: **While** flag= no **do**
3: Obtain $\mathbf{r}^{n^*}, \eta^{n^*}$ via solving the MILP master problem as outlined in (6a)-(6f)
4: Update $UB = \eta^{n^*}$
5: Given the first stage variables ($\mathbf{r}^{n^*}$), solve MILP sub-problem (7g)-(7j) and determine $\mathbf{u}^n$ and $\boldsymbol{\lambda}^n$
6: Update $LB = \max\left\{LB, \phi\left(\mathbf{r}^{n^*}, \mathbf{u}, \mathbf{q}\right)\right\}$
7: **If** $\left|UB - LB\right| \le \varepsilon$ **then**
8: flag=yes
9: **end if**
10: Create variables $\mathbf{q}^n$ and add (6d)-(6f) to the master problem
11: Update $O = O \cup \left\{S_n\right\}$
12: Update $n = n + 1$
13: **end while**
14: **return** $\mathbf{r}^{n^*}$

5. Numerical results

5.1. Case Study 1: IEEE 33-node distribution test system

The IEEE 33-node distribution test system [25] is used to validate the proposed MPS scheduling and MG forming. Numerical experiments are implemented in GAMS on a computer with an Intel i7-9750H, 2.59 GHz processor, and 16 GB of memory. The MILP master and sub-problems are solved by CPLEX solver.

As shown in Fig. 4, DSO faces 4 known branch damages after the disaster. Also, there are 3 unknown zones which are shown by rectangular boxes in the distribution system. According to the field crews' schedule, zones 1, 2, and 3 will respectively be inspected at hours 19, 7, 13 while the recovery process begins at hour 1. DSO expects to have the status of each zone branches at designated times. It is assumed that the charging capability in Depot 1 will be available from hour 4 on. The maximum estimated duration time of recovery process is adjusted to 24 h and time step is 1 h. There are 9 CLs assuming that they have the same importance except 3 of them, which are three times more critical than the others. They are called highly CLs. Emergency services, water stations, information and communication infrastructures, which have a direct impact on other interdependent critical infrastructures, can be defined as highly CLs [26]. Seven candidate nodes (stations) for placing 4 MPSs consisting of 3 truck-mounted mobile emergency generators and 1 truck-mounted mobile energy storage system are considered. It is assumed that all MPSs are placed in Depot 1 before the event. The MPSs and CLs characteristics are listed in Tables 1 and 2, respectively. In order to keep the results comparable and better show the impact of MPS charging capability, the initial charge level of MPS 4 is assumed to be 0. The goal is to maximize the sum of weighted restored CLs during 24 h recovery process (*i.e.* $\sum_t \sum_i \sum_l \alpha_i P_i^{l,t}$). In the proposed two-stage robust optimization approach, the budgets for all zones are set to 1 (i.e. $\Gamma_1 = \Gamma_2 = \Gamma_3 = 1$), which means 1 branch in each zone is maximally out of service after the inspection.

Five cases that dynamically schedule MPSs and form MGs are studied for comparison. The cases respectively are Deterministic Approach (DA) [12], Receding horizon Deterministic Approach (RDA), Robust Approach (RA), Receding horizon Robust Approach (RRA), and the Charging Receding horizon Robust Approach (CRRA). The properties of each case are presented in

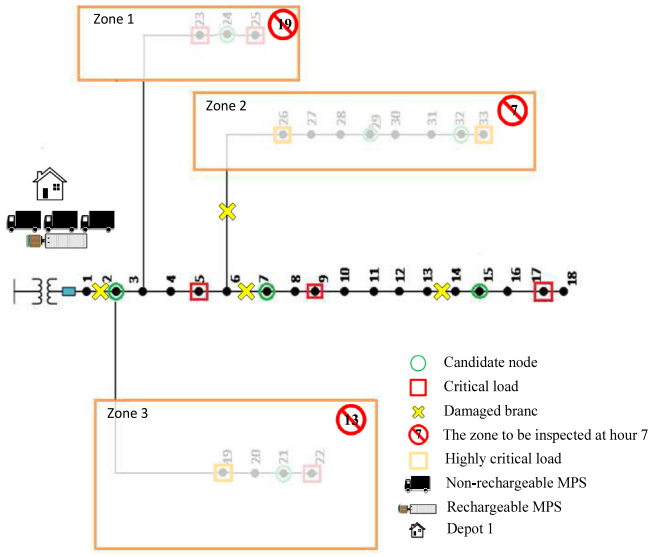

Fig. 4. IEEE 33-node distribution test system.

Table 1
CL parameters.

Node	P (kW)	Q (kvar)	Weight	Node	P (kW)	Q (kvar)	Weight
5	52.43	12.43	1	25	24.14	42.14	1
9	19.58	9.5	1	26	28.35	18.65	3
17	44.65	24.63	1	33	20.35	17.31	3
19	40.78	20.28	3	22	20.788	10.288	1
23	12.14	21.14	1	–	–	–	–

Table 2
MPS characteristics.

MPS	P_{dch}	Q_{dch}	Max. CHL (MWh)	Initial CHL %	η_{ch}/η_{dch}
MPS 1	125.33	64.25	2	85	−/0.95
MPS 2	196.23	86.52	2	85	−/0.95
MPS 3	92.63	54.56	2	85	−/0.95
MPS 4	92.63	54.56	0.5	0	0.95/0.95

Table 3
Each case properties.

Case	Uncertainties	Updating Data	Charging
DA	×	×	×
RDA	×	✔	×
RA	✔	×	×
RRA	✔	✔	×
CRRA	✔	✔	✔

Table 3. Note that both DA and RDA do not tackle uncertainty of branches status in the unknown zones. However, in RDA, new data associated with the branches is updated during recovery process and the model is re-optimized after each zone inspection.

In this part, a random scenario has been generated for showing each case performance. According to the scenario, branches 24–25, 30–31 and 21–22 will be declared damaged by field crews' inspections at mentioned hours. The resilience performance index (RPI) is defined as in (8) to show the performance of each approach under incomplete information. RPI is the ratio of the sum of weighted restored CLs under incomplete information divided by the sum of weighted restored CLs under complete information. In other words, the denominator corresponds to a situation in which all the uncertainties are known from the beginning of recovery state (t_r). In this test system, the denominator is equal to 6262.54 kWh and the nominator will be computed in each case.

$$RPI = \frac{\sum_t \sum_i \sum_l \alpha_i P_i^{l,t}\Big|_{\text{With incomplete data}}}{\sum_t \sum_i \sum_l \alpha_i P_i^{l,t}\Big|_{\text{With complete data}}} \times 100 \tag{8}$$

The simulation results and MPSs scheduling are given in Tables 4 and 5, respectively. In DA, neither the uncertainties nor new data has been taken into account. In this case, CLs 5, 19 and 17 are picked up by Nodes 2, 7 and 15, respectively. The objective function value is 2521.87 kWh, and the RPI is 40.27%. In the second case, RDA, the receding horizon framework is added to DA. At hours 7, 13, and 19, new data are received, and the model re-optimizes the decision variables over the remaining recover process. In comparison with DA restored loads, the highly CL 19 is also picked up by MPS 3 in Node 2 at hour 13. Thus, objective function value and RPI increase to 3969.07 kWh and 61.38%, respectively. As shown in Table 5, both DA and RDA have the same MPS scheduling, while RDA has picked up more load through network reconfiguration. Note that at hour 7, RDA cannot restore any of highly CLs 26 and 33 in Zone 2 because MPSs are not allowed to disrupt the restored CLs 5, 9, and 17. Also, MPS 3 is not able to pick up CL 23 at hour 19 due to its power capacity limitation. If MPS 1 had been positioned in Node 2 instead of MPS 3, it would have been able to pick up CL 23 at this hour. This weak utilization is due to neglecting the unknown zones at the beginning of the recovery state (t_r).

The third case, RA, considers the unknown zones by the two-stage robust optimization. The objective value and RPI are increased to 4225.57 kWh and 67.47%, respectively. As shown in Table 5, at first hours, MPS 3 is sent to Node 29 to restore one of highly CLs 26 or 33 depending on what scenario will happen in Zone 2. MPSs 1 and 2 are dispatched to Node 2. At hour 11, MPS 2 travels to Node 21. This strategy assures that CL 19 is survived by Nodes 2 or 21 regardless of which branch would be declared damaged. In contrast to RDA, Node 23 is picked up by MPS 1 at hour 19. MPS 1 in Node 2 has enough power capacity to serve CLs 5, 23, and highly CL 19, simultaneously. So compared to RDA, this case has positioned MPSs much better. However, RA has been solved just once at the beginning of recovery state, and decision variables have not been re-optimized then. As a result, MPS 2 in Node 21 is underutilized.

The fourth case, RRA, re-optimizes decisions using receding horizon framework as well as accommodating uncertainties. The objective function and RPI grow to 4775.02 kWh and 77.35%, respectively. The difference with RA is at hour 13. RRA re-optimizes decisions at hour 13 and sends MPS 2 toward Node 32 to survive highly CL 33. Note that in all four cases, the charging capability is not considered.

In the fifth case, CRRA, the charging capability is added to RRA. The objective function value and RPI are increased to 5712.67 kWh and 91.22%, respectively. As presented in Table 5, MPS 4 is being charged from hours 4 (earliest feasible charge time) to 11. Since this MPS is not available at the first periods, this approach uses it for areas which will be operable after inspections. This MPS picks up CL 33 in Zone 2. In addition to RRA restored CLs, CRRA has restored CL 17 from hour 4 so on by MPS 2. RPI of 91.22% means that the proposed model has performed 91.22%, similar to the case in which the information is complete at the beginning of the recovery process.

Figs. 5 and 6 show weighted restored loads and cumulative weighted restored energy for each five cases. Fig. 5 is monotonically increasing because DSO cannot interrupt the service, once a CL is restored (constraint (4h)). It can be observed that, at the early hours, the deterministic approaches have performed better than robust approaches. This greedy performance is due

Table 4
Simulation results for each case.

Case	Objective	RPI %	Restored loads %	Num. of Travels
DA	2521.87	40.27	32.82	3
RDA	3969.07	61.38	51.64	3
RA	4225.57	67.47	55.98	4
RRA	4775.02	77.35	60.93	5
CRRA	5712.67	91.22	73.13	5

Table 5
MPS scheduling for each case.

Time period	DA MPS 1	DA MPS 2	DA MPS 3	RDA MPS 1	RDA MPS 2	RDA MPS 3	RA MPS 1	RA MPS 2	RA MPS 3	RRA MPS 1	RRA MPS 2	RRA MPS 3	CRRA MPS 1	CRRA MPS 2	CRRA MPS 3	CRRA MPS 4
1																
2	*															
3	7		2	7		2	2	2			2		2			
4-11	** 7	15	2	7	15	2	2	2	29	2	2	29	2	15	29	Charging
12	7	15	2	7	15	2	2		29	2		29	2	15	29	
13	7	15	2	7	15	2	2	21	29	2	21	29	2	15	29	21
14-15	7	15	2	7	15	2	2	21	29	2		29	2	15	29	
16-24	7	15	2	7	15	2	2	21	29	2	32	29	2	15	29	32

* The symbol "⩛" shows this MPS is traveling on the transportation network.
** The number "7" means this MPS is positioned in Node 7.

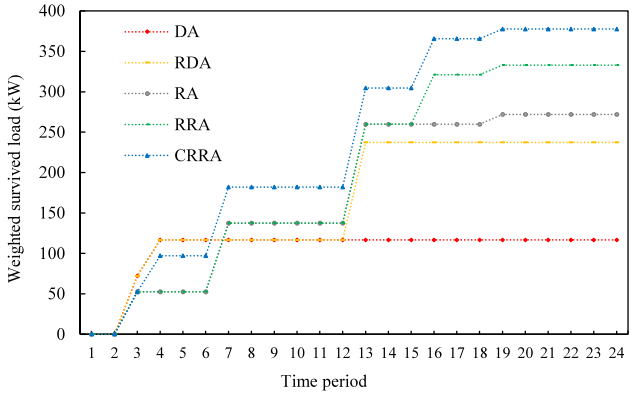

Fig. 5. Weighted restored load.

to the lack of insight over future uncertainties. However, as time goes on, robust approaches achieve higher objective functions. Comparing DA with RDA, it can be understood that the receding horizon has improved the objective function by re-optimizing the decision variables concerning operational constraints. By comparing RDA with RA and RRA, it is evident how having foresight into the uncertain future can improve the recovery performance. Finally, comparing RRA with CRRA demonstrates that charging capability in the robust receding horizon approach can effectively improve the recovery performance.

5.1.1. Statistical analysis

In order to validate performance of the proposed model, all branch damage scenarios are generated, and the sum of restored

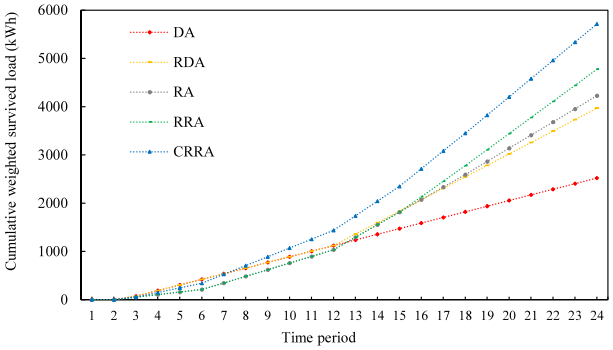

Fig. 6. Cumulative weighted restored energy.

CLs is calculated for each scenario. Simulation statistics are presented in Table 6. The proposed CRRA has achieved median objective function of 5596.21 kWh over all scenarios, and the median RPI over all scenarios is 88.58%. The results show that the proposed model, CRRA, has a remarkable overall performance. However, the deterministic approaches of DA and RDA have achieved weak median objective function of 2521.87 and 3562.47 kWh over all scenarios. It can be seen in Table 6 and Fig. 7, the standard deviations of robust approaches are considerably less than the deterministic approaches. As a result, the proposed model is reliable under incomplete information comparing to deterministic approaches. Furthermore, based on the estimated maximum number of damaged branches, the proposed robust model can assure a minimum objective function amount pertaining to the worst-case scenario at the beginning of the recovery state. At the first hour of the recovery state, the RA assures that at least 3720.73 kWh will be served until the end of recovery process. This amount is the minimum amount of RA objective function over all scenarios, as presented in Table 6. As it is evident in Table 6, the minimum amount of restored CLs in RRA has been increased by 250 kWh compared to RA. This improvement is happened due to implementing receding horizon framework. The median computation time of each approach, as well as the median number of iterations of the CC&G algorithm, is also presented in Table 6. It should be emphasized that the median computation time value for the proposed model is before the first inspection at the beginning of the recovery process with the highest uncertainty and the maximum estimated time horizon. The solution time of the proposed CRRA model is about 4 min for the 24 hours' recovery process, while the average computational times for the next inspection times are much less. For instance, the computational time for the last inspection is about 15 s. Compared to the time intervals of the receding horizon framework, all the computational times meet and outfit the performance requirements for the recovery state. Furthermore, the median number of iterations of the CC&G algorithm in the proposed CRRA is 5, which indicates a well enough convergence rate for the algorithm.

5.1.2. Uncertainty analysis

It is here shown that how increasing uncertainties affect performance of the proposed robust receding horizon-based recovery approach. DA and RRA are adopted for comparison, and the charging capability is neglected. The number of unknown zones is increased from 1 to 3. So, the number of uncertain branches increases as well. As demonstrated in Fig. 8, in case of existing uncertainty in Zone 1, RRA improves the deterministic performance by 8.88%. In the case of existing uncertainty in Zones 1, 2, and Zones 1, 2, 3, RRA improves the deterministic performance by

Table 6
Simulation results for robust optimization validation.

Method	Med. objective (kWh)	max. (kWh)	min. (kWh)	Std.	RPI %	Med. Iter.	Comp. Time
DA	2521.87	2521.87	2521.87	0	40.27	–	50 s
RDA	3969.07	4074.93	2521.87	605.94	61.38	–	80 s
RA	4225.57	4475.09	3720.73	241.97	67.47	6	2.5 min
RRA	4475.02	4775.02	3970.18	268.3	73.26	4	3 min
CRRA	5412.02	5712.02	4907.18	245.65	89.65	5	4 min

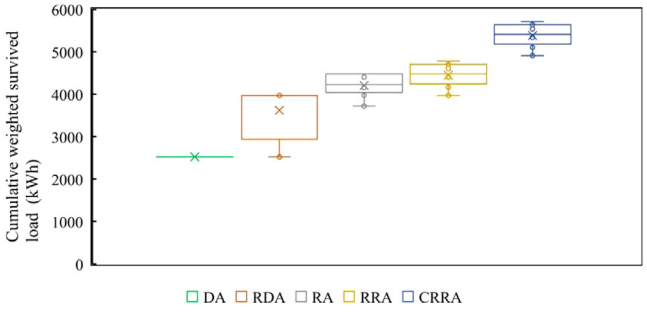

Fig. 7. Statistical analysis of various scenarios.

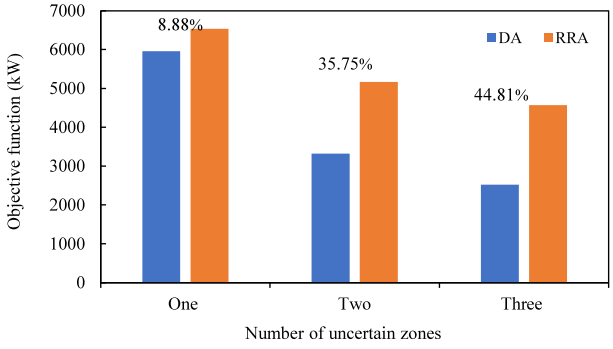

Fig. 8. Uncertainty analysis.

Table 7
CLs parameters.

Node	P (kW)	Q (kvar)	Weight	Node	P (kW)	Q (kvar)	Weight
1	41.79	21.29	3	46	28.35	18.65	3
9	52.43	12.43	1	66	20.35	17.31	1
17	19.58	9.5	1	94	20.08	14.25	1
27	44.65	24.63	1	87	26.75	44.56	3
30	40.78	20.28	1	79	14.56	42.52	1
37	12.14	21.14	1	101	33.71	13.25	1

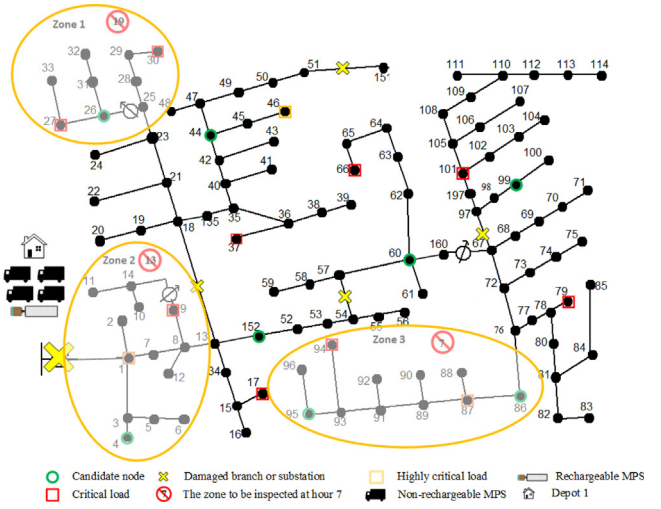

Fig. 9. IEEE 123-node test feeder.

35.75 and 44.81%, respectively. In summary, as the number of unknown zones or uncertain branches increases, which is prevalent in high-impact disasters, the proposed model can achieve better decisions and restore the higher amount of load demand. Also, re-optimizing the decisions by receding horizon framework can better capture uncertainties when updated data is received.

5.2. Case Study 2: IEEE 123-node test feeder

In order to show the replicability and scalability of the proposed model, the IEEE 123-node test feeder is utilized [27]. The known branch damages, CLs and candidate nodes locations are based on the data given in [11]. Also, to increase the complexity of the problem, three more candidate nodes and one more CL is added to the distribution system. The CLs characteristics are given in Table 7. As can be seen, three of the CLs have higher weights and are assumed as highly CLs. Furthermore, eight candidate nodes are considered for placing 5 MPSs. It is assumed that all MPSs are placed in Depot 1 before the event. The MPSs characteristics are the same as the previous case study which are listed in Table 1 (we have 2 of MPS 1). As shown in Fig. 9, DSO faces 4 known branch damages and 3 unknown zones after the disaster. According to the field crew's schedule, zones 1, 2, and 3 will respectively be inspected at hours 19, 13 and 7 while the recovery process begins at hour 1. Charging capability is available at the beginning of the process in Depot 1, and the budgets are $\Gamma_1 = 2$, $\Gamma_2 = \Gamma_3 = 1$.

In order to show the effectiveness of the proposed method (CRRA), a comparison with [12] is carried out. Note that charging capability is added to DA in [12] to create a similar condition. Furthermore, a benchmark is devised to validate the proposed robust receding horizon methodology. The benchmark dispatches the MPSs and forms multiple MGs in the distribution system with complete information about the unknown zones at the beginning of the recovery process. The damage scenario in unknown zones is considered in such a way that the benchmark objective function value has the most difference with the proposed model. In fact, in this scenario, the proposed model has the lowest performance compared with the benchmark. According to this scenario, branches 1–3, 87–86, 26–27 and 26–31 will be declared damaged by the field crews' inspections at mentioned hours.

The weighted restored load and cumulative weighted restored energy for each case are shown in Figs. 10 and 11, respectively. It can be observed from Fig. 10 that the DA does not follow the benchmark curve. This weak performance is due to the lack of insight into future uncertainties. Also, it cannot re-optimize the decisions after receiving new data which exacerbates its performance. Although DA shows slightly better performance at early hours owing to its greedy performance, the proposed approach is able to restore more weighted CLs over the recovery process.

By taking the uncertainties into account in the two-stage robust optimization approach, the proposed model is able to pick up the highly CL 87 in zone 3. Given the MPS scheduling in Table 8,

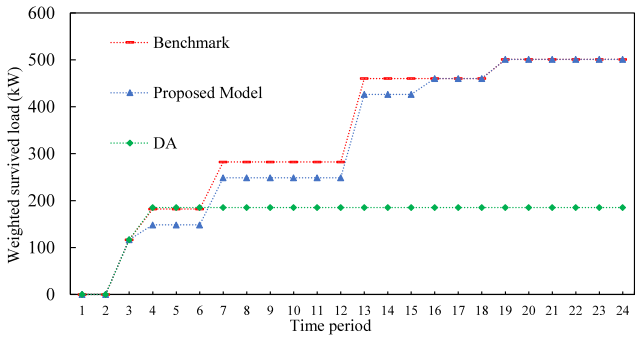

Fig. 10. Weighted restored load.

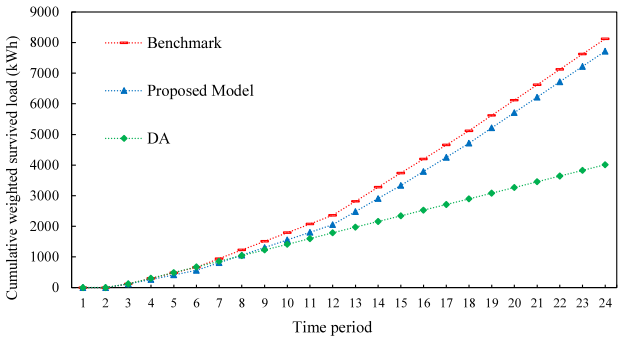

Fig. 11. Cumulative weighted restored energy.

MPS 4 is sent to Node 95 after charging, and it arrives at hour 7. Because MPS 2 is positioned in Node 60 at that time, two paths are created to restore highly CL 87. After the inspection of zone 3 at hour 7, branch 86–87 is declared damaged. As a result, it cannot restore the highly CL 87 by Node 60. So, the model restores it by MPS 4 which is in Node 95. This strategy actually assures that this highly CL can be picked up and shows how the proposed robust approach is capable of restoring highly CLs while considering the uncertain branch damages. Furthermore, in order to restore CL 9 and highly CL 1 in zone 2, MPS 3 is sent to Node 4. This strategy creates two paths to pick up these two CLs (from both Node 152 and 4). After branch 1–3 declared damaged, it restores both CL 19 and highly CL 1 by MPS 5 in Node 152. MPS 4 in Node 4 is now underutilized. Thanks to the receding horizon framework, the decisions are re-optimized and MPS 4 is sent to Node 99 to pick up CL 101 at hour 16. However, the benchmark has picked up CL 101 earlier at hour 4. This is due to having complete data about uncertain branches in unknown zones.

As given in Table 9, the DA has restored 4009.96 kWh weighted CLs and the RPI is 49.23%. In the proposed model, the objective function value and RPI are increased to 7719.18 kWh and 95.02%, respectively. Recall that in this scenario, the proposed method has the lowest objective function value compared to the benchmark. Therefore, the RPI of 95.02% in this worst-case scenario clearly shows the reliability and effectiveness of the proposed model. Also, it is obvious that even if the receding horizon approach was added to DA, it would perform much weaker than the proposed model due to the lack of insight over the uncertain future. This comparison is made in the previous case study by comparing RDA and RRA, and it is neglected here to avoid redundancy.

As the computation time in Table 9 reveals, a fourfold increase in the size of the test system compared with the IEEE 33-node test system only results in a 2.5-fold increase in the computation time. Note that the two other approaches have less computation time compared with the proposed model since they do not take the branches uncertainties into account. Also, the number of iterations of the proposed model indicates an appropriate convergence rate of the CC&G algorithm in the case of real-scale systems.

Table 8
MPS scheduling for each case.

	Time period						
	1	2	3	4	5-6	7-13	14-15	16-24
DA								
MPS1	POT1	→*	Node 60					
MPS2	POT1	→	Node 44					
MPS3	POT1	→	Node 99					
MPS4	POT1	Charging		→	Node 44			
MPS5	POT1	→	Node 152					
Proposed Model								
MPS1	POT1	→	Node 44					
MPS2	POT1	→	Node 60					
MPS3	POT1	→	Node 4			→	Node 99	
MPS4	POT1	Charging			→	Node 95		
MPS5	POT1	→	Node 152					
Benchmark								
MPS1	POT1	→	Node 44					
MPS2	POT1	→	Node 60					
MPS3	POT1	→	Node 99					
MPS4	POT1	Charging			→	Node 95		
MPS5	POT1	→	Node 152					

Table 9
Simulation results for each case.

Method	Objective (kWh)	RPI %	Computation time (min)	Iter.
DA [12]	4009.96	49.23	2.5	–
Proposed Model	7719.18	95.02	8.5	5
Benchmark	8123.7	100	3	–

6. Conclusion

In this paper, a robust receding-horizon based recovery framework was presented for scheduling MPSs and forming MGs while maximizing the weighted sum of restored CLs. Simulation results showed that incomplete information in the deterministic approach led to MPS underutilization and weak recovery performance. However, considering unknown zones and re-optimizing the decision variables with respect to the updated data received from field crews' inspections can significantly increase the sum of restored CLs. Furthermore, the charging capability of mobile energy storage systems under incomplete information significantly improves recovery performance and system flexibility during the long-lasting services. It is observed that as the level of uncertainty increases, the proposed model further outperforms the deterministic approach. Also, the simulation results support scalability and performance of the proposed model in large-scale systems. The extension of the proposed methodology to accommodate the lateral objectives such as loss reduction within the restoration process or revising the MG formation and MPSs positioning solution in accordance with the succeeding epochs of the extended extreme events can be investigated by future research endeavors.

CRediT authorship contribution statement

Seyed Amin Sedgh: Writing - original draft, Software, Conceptualization. **Meysam Doostizadeh:** Methodology, Formal analysis, Software, Visualization. **Farrokh Aminifar:** Validation, Writing - review & editing, Supervision. **Mohammad Shahidehpour:** Validation, Writing - review & editing.

Declaration of competing interest

The authors declare that they have no known competing financial interests or personal relationships that could have appeared to influence the work reported in this paper.

References

[1] A. Gholami, T. Shekari, M.H. Amirioun, F. Aminifar, M.H. Amini, A. Sargolzaei, Toward a consensus on the definition and taxonomy of power system resilience, IEEE Access 6 (2018) 32035–32053.

[2] M. Panteli, P. Mancarella, The grid: stronger bigger smarter?, IEEE Power Energy Mag. 13 (3) (2015) 58–66.

[3] C. Chen, J. Wang, D. Ton, Modernizing distribution system restoration to achieve grid resiliency against extreme weather events: an integrated solution, Proc. IEEE 105 (7) (2017) 1267–1288.

[4] S. Lei, C. Chen, H. Zhou, Y. Hou, Routing and scheduling of mobile power sources for distribution system resilience enhancement, IEEE Trans. Smart Grid 10 (5) (2019) 5650–5662.

[5] S. Thakar, A.S. Vijay, S. Doolla, System reconfiguration in microgrids, Sustain. Energy. Grids Netw. 17 (2019) 100191.

[6] J. Ebrahimi, M. Abedini, M. Mahdi, Optimal scheduling of distributed generations in microgrids for reducing system peak load based on load shifting, Sustain. Energy. Grids Netw. 23 (2020) 100368.

[7] A.H. Hubble, T.S. Ustun, Composition, placement, and economics of rural microgrids for ensuring sustainable development, Sustain. Energy. Grids Netw. 13 (2018) 1–18.

[8] A. Hussain, V.H. Bui, H.M. Kim, Microgrids as a resilience resource and strategies used by microgrids for enhancing resilience, Appl. Energy 240 (2019) 56–72.

[9] A. Khodaei, Provisional microgrid planning, IEEE Trans. Smart Grid 8 (3) (2017) 1096–1104.

[10] H. Farzin, M. Fotuhi-Firuzabad, M. Moeini-Aghtaie, Enhancing power system resilience through hierarchical outage management in multi-microgrids, IEEE Trans. Smart Grid 7 (6) (2016) 2869–2879.

[11] S. Poudel, A. Dubey, Critical load restoration using distributed energy resources for resilient power distribution system, IEEE Trans. Power Syst. 34 (1) (2019) 52–63.

[12] S. Lei, J. Wang, C. Chen, Y. Hou, Mobile emergency generator pre-positioning and real-time allocation for resilient response to natural disasters, IEEE Trans. Smart Grid 9 (3) (2018) 2030–2041.

[13] L. Che, M. Shahidehpour, Adaptive formation of microgrids with mobile emergency resources for critical service restoration in extreme conditions, IEEE Trans. Power Syst. 34 (1) (2019) 742–753.

[14] S. Yao, P. Wang, T. Zhao, Transportable energy storage for more resilient distribution systems with multiple microgrids, IEEE Trans. Smart Grid 10 (3) (2019) 3331–3341.

[15] S. Lei, C. Chen, Y. Li, Y. Hou, Resilient disaster recovery logistics of distribution systems: Co-optimize service restoration with repair crew and mobile power source dispatch, IEEE Trans. Smart Grid 10 (6) (2019) 6187–6202.

[16] Y. Xu, Y. Wang, J. He, M. Su, P. Ni, Resilience-oriented distribution system restoration considering mobile emergency resource dispatch in transportation system, IEEE Access 7 (2019) 73899–73912.

[17] A. Kavousi-Fard, M. Wang, W. Su, Stochastic resilient post-hurricane power system recovery based on mobile emergency resources and reconfigurable networked microgrids, IEEE Access 6 (2018) 72311–72326.

[18] S. Yao, P. Wang, X. Liu, H. Zhang, T. Zhao, Rolling optimization of mobile energy storage fleets for resilient service restoration, IEEE Trans. Smart Grid 11 (2) (2019) 1030–1043.

[19] J.C. Bedoya, J. Xie, Y. Wang, X. Zhang, C.-C. Liu, Resiliency of distribution systems incorporating asynchronous information for system restoration, IEEE Access 7 (2019) 101471–101482.

[20] G. Zhang, J. Lu, J. Montero, Y. Zeng, Model, solution concept, and Kth-best algorithm for linear trilevel programming, Inf. Sci. (Ny). 180 (4) (2010) 481–492.

[21] A. Gholami, T. Shekari, S. Grijalva, Proactive management of microgrids for resiliency enhancement: An adaptive robust approach, IEEE Trans. Sustain. Energy 10 (1) (2019) 470–480.

[22] M.H. Amirioun, F. Aminifar, H. Lesani, Resilience-oriented proactive management of microgrids against windstorms, IEEE Trans. Power Syst. 33 (4) (2018) 4275–4284.

[23] M.H. Taheri, S. Dehghan, M. Heidarifar, H. Ghasemi, Adaptive robust optimal transmission switching considering the uncertainty of net nodal electricity demands, IEEE SYST J. 11 (4) (2017) 2872–2881.

[24] B. Zeng, L. Zhao, Solving two-stage robust optimization problems using a column-and-constraint generation method, Oper. Res. Lett. 41 (5) (2013) 457–461.

[25] M.E. Baran, F.F. Wu, Network reconfiguration in distribution systems for loss reduction and load balancing, IEEE Trans. Power Deliv. 4 (2) (1989) 1401–1407.

[26] J.R. Marti, E. Ghahremani, A. Marti, The GDW index: An extension of the GDP index to include human well-being, Eur. CIIP Newsl. 10 (2) (2016) 23–26.

[27] The IEEE 123-node test feeder. [Online]. Available: https://site.ieee.org/pes-testfeeders/resources/.